Calculations of Field Distribution and SAR in Interventional MR: A Pilot Study

Oliver Wieben, Susan Hagness

Abstract— **This project describes a pilot study for safety issues in interventional Magnetic Resonance Imaging (MRI). A literature review surveys the components involved in such a system and analytical and numerical solutions for the time varying magnetic and electric field distributions during normal MR scans. The safety aspects of active catheter tracking in interventional MR are investigated in terms of a numerical simulation. A 2D FDTD algorithm analyzes the effects of the coil on the specific absorption rate in an interventional MR experiment in the presence of a catheter with an electric antenna for the active tracking of the catheter localization.**

Keywords— **Magnetic Resonance Imaging, Interventional MR, Active Catheter Tracking, Numerical Method, Specific Absorption Rate.**

I. Introduction

RECENT advances in MR system design resulted in an increased interest in the usage of MR scanners for interventional procedures. The MR images can be used for guidance of minimally invasive surgery (RF ablation, insertion of stents, etc.). The advantages of a MR system versus the gold standard of x-ray fluoroscopy include the avoidance of exposure to radiation for the patient and surgery team, the availability of 3D information and functional data (perfusion of tissues, temperature maps, etc.), and higher soft tissue contrast.

A promising approach for real-time tracking of a catheter is the insertion of a coil in the tip of the catheter, which can be used as a receiving coil during an MR procedure. Potential problems with this approach are distortions of the magnetic field heating of the coil. Perturbations of the magnetic field can decrease the image quality and increase the specific absorption rates (SAR) of the rf energy. The heating of the catheter can irreversibly damage the surrounding tissue.

Although multiple authors have expressed concern about this heating problem and some have performed measurements on phantoms, no analytical or numerical simulations have been performed to our knowledge. This work is intended as a pilot study for the feasibility of the FDTD [1], [2] algorithm to simulate the physical processes involved. A perfect numerical simulation of the problem described above would include:

- a geometric model of the human body (mm^3)
- a finer geometric model of the catheter (10^{-2} mm^3)
- a geometric model of the birdcage coil (mm^3)
- a physical model of the current distribution in the coil
- derivations of the heat in the catheter-coil
- modeling of the heat transfer catheter-coil to tissue incl. blood flow.

The implementation of a perfect simulation of this problem is beyond the scope of this project. We will discuss the individual components of the system and describe the implementation of a 2D FDTD algorithm with a simple homogeneous tissue sample and a simple antenna geometry.

Oliver Wieben is with the Departments of Electrical and Computer Engineering, Medical Physics, and Radiology at the University of Wisconsin–Madison. E-mail: wieben@mr.radiology.wisc.edu .

II. Background Information

The implementation of a numerical simulation requires detailed knowledge about the components of the simulated system. This section is devoted to the introduction and characterization of the most important components for an interventional procedure on a MR scanner.

A. Tissue Model

The generation of an anatomically and physically correct model of the human body is a very challenging task. Such models are desirable for educational purposes, and for simulations of all kinds, including mechanical simulations (e.g. human gait, heart valves, prostheses), electromagnetic simulations (e.g. rf penetrations into the human body, electric defibrillation of the heart, electrical stimulation of muscles and nerves, rf ablation of tissue, microwaves for breast cancer detection), and heat transfer simulations (e.g. thermotherapy, rf ablation).

Data from medical imaging devices such as ultrasound, CT, or MR are used often to generate such models. The National Institute of Health sponsored the *Visible Human Project*, which provides all of these data sets and color photographs of the according slices through a male and a female body. The highest resolution in these data is 1 mm^3. Classification algorithms are used to differentiate between tissues and then the properties of interest (e.g. stress modules, heat capacities, or conductivity and magnetic susceptibility) are assigned to the identified tissues. Generally, these properties can vary with the orientation of the tissue, temperature, and other parameters for example the wavelength in electromagnetic simulations.

B. Static Magnetic Field B_0

In MR imaging, the patient is exposed to a strong static magnetic field B_0 (commonly 1.5 Tesla = 15,000 Gauss). This field is generated by a high currents in a superconducting solenoidal coil. This fields is referred to as the B_0 field and aligns with the body axis when the patient lies in the scanner. The axis of the B_0 field is the z axis in our coordinate system. Atoms that possess a magnetic spin align in certain energy states with this strong exterior magnetic

field. The spins resonate at the so called Larmor frequency f_0, which is given as

$$f_0 = \frac{\gamma}{2\pi}|\vec{B_0}|, \tag{1}$$

where γ is the atom specific gyromagnetic ratio. The most commonly used atom in medical MR imaging is the proton ($\gamma = 267.53$ MHz/T).

C. Time Varying B_1-Field

During the imaging procedure an additional time varying B_1 field is generated perpendicular to the static field. This additional field is necessary to excite the magnetic spins (hydrogen protons) which are the signal source for MR imaging. The B_1 field has to oscillate with the Larmor frequency f_0 of the spins. Therefore, the excitation of the spins requires a RF pulse with a frequency centered at 63.87 MHz. A discussion of the MR phenomena and the underlying principles for the image reconstruction can be found in standard references [3], [4], [5].

The duration of the B_1 pulse T_{rf} may vary between $\approx 400\mu$s and ≈ 4 ms and is fairly small compared to the main magnetic field ($\approx 20\ \mu\text{T} = 0.2$ Gauss). These pulses are either generated as a hard pulse (the sinusoidal wave is multiplied with a rectangular function) or a soft pulse (the sinusoidal wave is multiplied with a sinc function).

D. Birdcage Coil Design

The MR system requires a transmit coil for the generation of the B_1 field with an rf pulse and a coil to receive the echo signal from the magnetic spins. Since transmission and receiving never occurs at the same time, one coil can be used to fulfill both purposes.

The most common coil design for the B_1 field is the birdcage coil. This coil was introduced by Hayes in 1985 [6], [7]. Its advantage is a highly uniform magnetic field inside the coil. The birdcage coil consists of N rods, which are organized in a circular fashion and connected by two end rings. Figure (1) shows the geometry of such a design. In the simplest mode, two opposite rods are used as the terminals of a current supply $I_s(t) = \hat{I}_s \sin(2\pi f_0 t)$. Capacitors in between the rods on the end rings introduce a phase difference in the currents in the rods [8], [9]. Ideally, the current distribution in the rods is

$$\begin{aligned} I_n(t) &= I_s(t)\sin(2\pi(n-1)/N) &(2)\\ &= \hat{I}_s \sin(2\pi f_0 t)\sin(2\pi(n-1)/N), &(3)\end{aligned}$$

where $1 \le n \le N$.

E. Catheter Design

An interventional procedure is typically performed by inserting a catheter into one of the the femural arteries (upper leg). From there the catheter can be steered under guidance of the imaging system into almost all parts of the vascular system. Therefore, the catheters are designed to be fairly small in diameter (leq 1 mm). Typically, interventional procedures are performed with X-ray fluoroscopy systems.

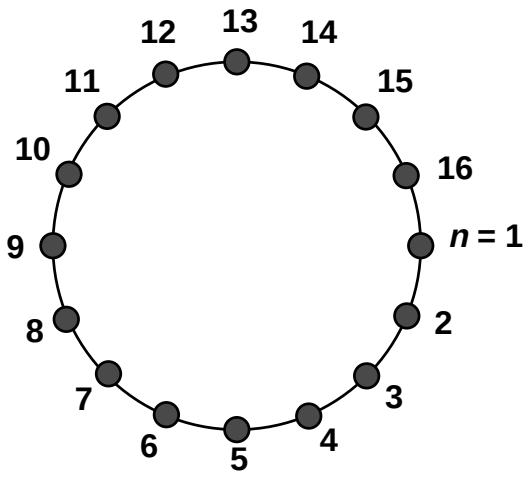

Fig. 1. The concept of the birdcage design. A cut in the $x-y$ plane is shown. Each rod carries the source current density with a sinusoidal weighting pattern: $I_n(t) = I_s(t)\sin(2\pi(n-1)/N) = \hat{I}_s \sin(2\pi f_0 t)\sin(2\pi(n-1)/N)$. The most common implementation is shown with $N = 16$.

Only recent advances in MR technology have encouraged research in the usage of MR scanners for similar procedures [10]. Among different approaches for the catheter localization, active catheter tracking is the most popular [11], [12]. With this technique, a small receiver coil is placed on the tip of the catheter and connected with 2 leads to an amplifier at the end of the approximately 2m long catheter.

F. Patient Safety in MRI

The are some parameters in MR imaging that have to be considered for patient safety [13]. We will concentrate here on safety aspects related to the rf pulses during an MR exam. The birdcage coils are designed to maximize field homogeneity in the coil volume (important for image quality) and to minimize the electric field to minimize the energy deposited in the patient. However, the loading of the coil with different patient sizes deteriorates the homogeneity of the B_1 field and causes increased energy depositions, especially for high field MR imaging when the size of the imaged object becomes comparable to the effective wavelength.

The first approximations of field homogeneity and power deposition for MR experiments were done with analytical approaches. Foo et al. [14], [15] solved a 3D model with cylindrical geometry of a homogeneous body. They modeled the birdcage coil and discuss coil design issues at different field strengths. Jin et al. [16] presented a 2D mathematical model for the field inhomogeneity of unloaded birdcage coils. Simunic et al. [17] implemented a Finite Element Method (FEM) to investigate hot spots of SAR in a human head model. This model is superior to a homogeneous model although it suffers from a low spatial resolution (3256 voxels and 11 tissue classes). A fast 2D analysis based on a finer model was presented by Jin et al. [18]. The same group implemented a 3D-FDTD algorithm for the analysis of SAR and field homogeneity. They em-

bedded the method of moment (MoM) to determine the current distribution in the coil with a so called lumped-circuit method.

The study of heating effects is of special interest in the presence of metallic objects in the body, which are excellent conductors and do perturb the electric field. Studies have been performed on heating of EKG electrodes [19] and metallic implants [20]. Some authors have expressed concern about the heating effects during interventional MR procedures with active catheter tracking [21]. Maier et al. [22] have acquired some temperature measurements from a phantom scan.

III. Methods

The distribution of the magnetic and electric field components were investigated with the FDTD algorithm in the 2D-TM mode.

A. FDTD Algorithm

The update equations for the field components are derived from the Yee algorithm. The magnetic field components are given by:

$$\begin{aligned} H_x|^{n+1/2}_{i+1/2,j} &= D_A H_x|^{n-1/2}_{i+1/2,j} \\ &- D_B \left[E_z|^n_{i+1/2,j+1/2} - E_z|^n_{i+1/2,j-1/2} \right] \end{aligned} \tag{4}$$

and

$$\begin{aligned} H_y|^{n+1/2}_{i,j+1/2} &= D_A H_y|^{n-1/2}_{i,j+1/2} \\ &- D_B \left[E_z|^n_{i+1/2,j+1/2} - E_z|^n_{i-1/2,j+1/2} \right], \end{aligned} \tag{5}$$

where $D_A = 1$ and $D_B = \frac{\Delta t}{\mu \Delta x}$.

The update equation for the electrical field component E_z is slightly modified as compared to the simple FDTD algorithm to incorporate the conductivity of the phantom and the external current J_{ext} in the coil rods.

$$\begin{aligned} E_z|^{n+1}_{i+1/2,j+1/2} &= C_A E_z|^n_{i+1/2,j+1/2} \\ &+ C_B \left[H_y|^{n+1/2}_{i+1,j+1/2} - H_y|^{n+1/2}_{i,j+1/2} \right] \\ &- C_B \left[H_x|^{n+1/2}_{i+1/2,j+1} - H_x|^{n+1/2}_{i+1/2,j} \right] \\ &- C_C J_z|^n_{i+1/2,j+1/2} \end{aligned} \tag{6}$$

where

$$\begin{aligned} C_A &= \frac{1 - \frac{\sigma \Delta t}{2\epsilon}}{1 + \frac{\sigma \Delta t}{2\epsilon}} \\ C_B &= \frac{\frac{\Delta t}{\epsilon \Delta x}}{1 + \frac{\sigma \Delta t}{2\epsilon}} \\ C_C &= \frac{\frac{\Delta t}{\epsilon}}{1 + \frac{\sigma \Delta t}{2\epsilon}}. \end{aligned} \tag{7}$$

B. Grid Geometry

The field components in the simulation vary with the frequency f_0. The duration for one cycle is $T_0 = 1/f_0 = 1.57$ ns and corresponds to a wavelength in free space $\lambda_0 = \frac{c_0}{f_0} = 4.69$ m. A minimum length Δx_{min} of the grid cells is required. A typical value is given by

$$\Delta x_{min} \leq \frac{c_0}{f_0 20 \sqrt{\epsilon_r}}. \tag{8}$$

This corresponds to a length $\Delta x_{min} = 0.23$ m for a simulation in free space only and to a length $\Delta x_{min} = 0.023$ m for a simulation including a material with $\epsilon = 100$. Since we are interested in a fine resolution of the resulting field, a length of $\Delta x = \Delta y = 0.01$ m was chosen. The minimum duration for the time steps was chosen as $\Delta t = \frac{\Delta x}{\sqrt{2} c_0} = 23.6$ ps. In other words, the simulation of one cycle requires $T_0/\Delta t = 664$ time steps.

The body birdcage coil has a diameter of 0.6 m and about the same length. The 2D plane for the simulation represents a slice perpendicular to the axis of the coil. We simulated a birdcage coil with $N = 16$ rods because it is the most commonly used coil. The covered area for the simulation was 0.8×0.8 m with the coil centered in this area. With this geometry, we have 79×79 electric field components E_z, 79×80 magnetic field components H_x, and E_z, 80×79 magnetic field components H_y.

In a second experiment, a material was added to mimic the presence of tissue in the coil. Foo et al. [14] used a homogeneous cylinder with $\epsilon_r = 58$ and $\sigma = 0.3$ S/m to represent an equivalent body load. Comprehensive studies of these parameters for different tissues over a wide frequency range were performed by Gabriel et al. [23], [24], [25].

C. Source Waveform

The current density as a function of the rod and time is given by equation 2. It is not advisable in a numerical simulation to switch on a source waveform like a hard pulse ($J_n(t) = \hat{J}_s \sin(2\pi f_0 t) \sin(2\pi(n-1)/N) u(t)$). Instead a ramp for a transient increase in the field component is desired to avoid high frequency components. This can be accomplished by the multiplication of a transient such as an exponential or Gaussian function:

$$J'_n(t) = (1 - \exp^{-t\alpha}) J_n(t) \tag{9}$$

A typical value for α is $5/(2\pi f_0$ [26]. This corresponds to a full magnitude of the excitation after 3 periods T_0. It would require ≈ 2000 iterations in our simulation to reach $t = 3T_0$. I chose $\alpha = 1/(10\pi f_0)$ to decrease this warm-up period since the used Δt is so small.

D. Boundary Conditions

The boundary condition on the grid boundaries were implemented with the second order MUR radiation boundary condition. This boundary is designed to absorb the incoming wave with minimal reflections. Such a boundary simulates propagation into free space which resembles the physical presence of a rf shield around the birdcage coil. An alternative boundary condition would be the PML ABC (perfectly matched layer absorbing boundary condition).

E. SAR

The specific absorption rate SAR characterizes the dose of absorbed rf energy during an MR examination. It is derived as

$$SAR = \frac{Q}{\rho} = \frac{\sigma|\vec{E}|^2}{2\rho}. \tag{10}$$

For biological tissues, the density can be estimated to be equal to water ($\rho_{water} = 1$ g/cm^3). Therefore, we derive:

$$SAR = \frac{\sigma(E_x^2 + E_y^2 + E_z^2)}{2} \tag{11}$$

for a given electrical field. In our implementation, the E-field has a z component only. The total absorbed energy in an MR exam can be derived from the calculated SAR by multiplication with $\frac{n_{rf}T_{rf}}{T_{exam}}$, where n_{rf} is the number of rf pulses applied and T_{exam} is the total duration of the exam. Typical values are $n_{rf}T_{rf} = 4.7$ s and $T_{exam} = 6$ minutes.

IV. Results

A. Linear Polarized B_1-Field

For the first experiment, we investigated the electric and magnetic field components for a linear polarized field. The coil was unloaded and excited by a current as given by equation 2. We analyzed the $\vec{H}$-field which is related to the $\vec{B}$ field by $\vec{B} = \mu\vec{H}$. The field sourced by the coil currents results in a fairly homogeneous region in the center of the coil. The magnetic field has effectively only one component: H_x. The H_y component is negligible and the magnetic field is

$$\vec{H}(t) = \hat{H}\cos(2\pi f_0 t)\vec{e}_x \tag{12}$$

or, in complex notation

$$H(t) = \frac{\hat{H}}{2}(\exp^{j2\pi f_0 t} + \exp^{-j2\pi f_0 t}). \tag{13}$$

The complex notation shows, that the linear polarized field can be represented by 2 rotating fields. Only the components rotating with the magnetic spins is effective in tipping the magnetization in the transverse plane for the MR experiment. The other component is off resonance.

The resultant E-field is just represented by the E_z component. The amplitude $\hat{E}$ of the sinusoidal field component can be derived from the observation of one cycle after the steady state is reached. The results of the numerical simulation are shown in Figure (2). The magnitude of the components was derived by setting the magnetic field in the center of the grid to 21.49 A/m. All other values can be derived from this. The magnetic field has two components and therefore the final component represented in Figure (2) is $\hat{H} = \sqrt{\hat{H}_x^2 + \hat{H}_y^2}$ component. Note, that in all presented images the maximum represented value was set to 10 V/m for the electric field (red color) and to 40 A/m (31.9 μT).

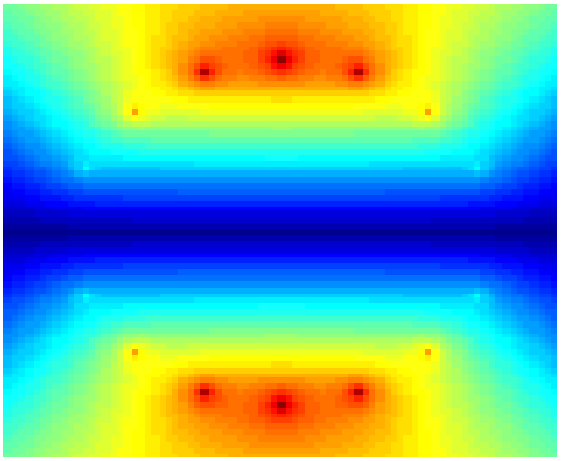

(a)

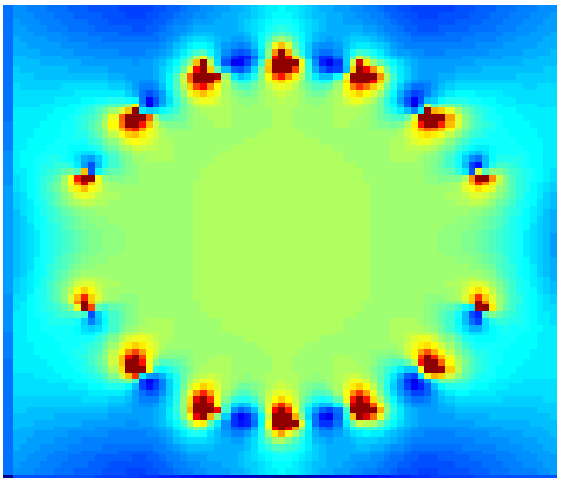

(b)

Fig. 2. The electric field (a) and the magnetic field (b) of an unloaded birdcage coil with a linear excitation.

B. Circular Polarized B_1 Field

A more effective usage of the magnetic field is achieved with a circular polarized field. This can be achieved by using the same geometry as for the linear field and superimposing a second one, that creates a linear field in the y-direction. If both components are $\pi/2$ out of phase [27], we have

$$\vec{H}_x(t) = \hat{H}\cos(2\pi f_0 t)\vec{e}_x \tag{14}$$
$$\vec{H}_y(t) = \hat{H}\sin(2\pi f_0 t)\vec{e}_y \tag{15}$$
$$\tag{16}$$

or, in complex notation

$$H(t) = \hat{H}\exp^{j2\pi f_0 t} \tag{17}$$

A comparison of linear and circular polarized fields can be found in [28]. A circular polarized bird coil is driven

by two pairs of terminals which are perpendicular to each other. This coil mode is referred to as quadrature mode. The results of the simulation were scaled to achieve a magnetic field strength of 15.2 A/m, which is equivalent to the magnitude for the linear field divided by $\sqrt{2}$. The results of the simulation are shown in Figure (3)

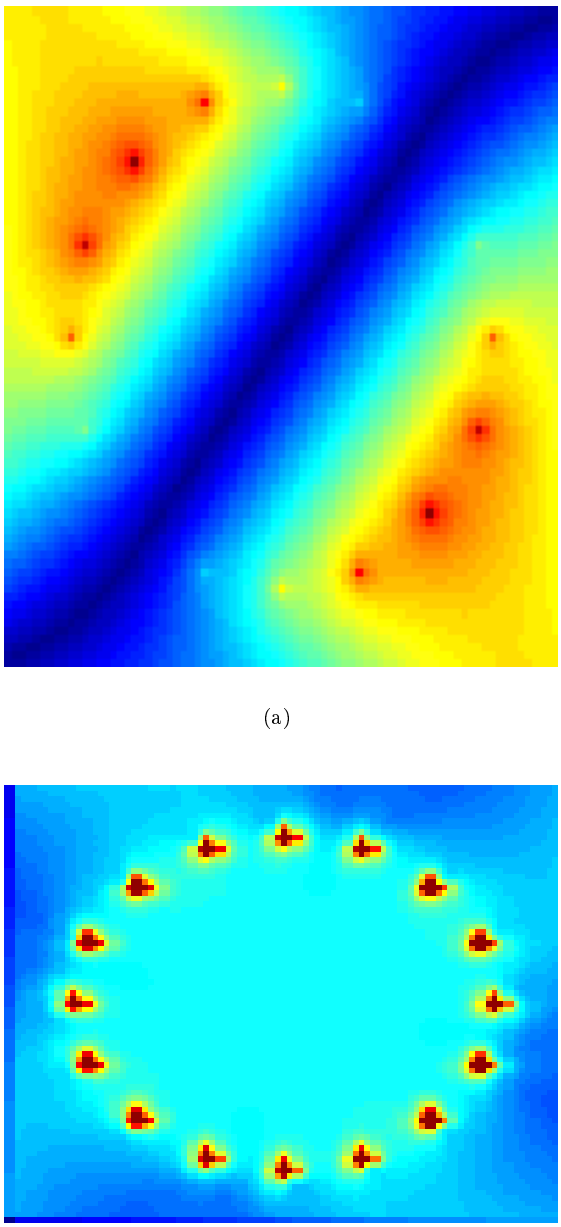

(a)

(b)

Fig. 3. The electric field at a snapshot in time (a) and the magnetic field (b) of an unloaded circular birdcage coil. The axis of the electrical field rotates around the center of the grid.

We see that the electric field is symmetric to the center of the grid with a circular excitation. The homogeneity of the field is increased as compared to the linear excited field.

C. Loaded Coil

In this experiment, the coil was not only filled with air, but also with a homogeneous material in the center of the coil. The diameter of the material mimicking the presence of a human body in the scanner was chosen as 36 cm. The magnetic field and the SAR map are shown in Figure (4)

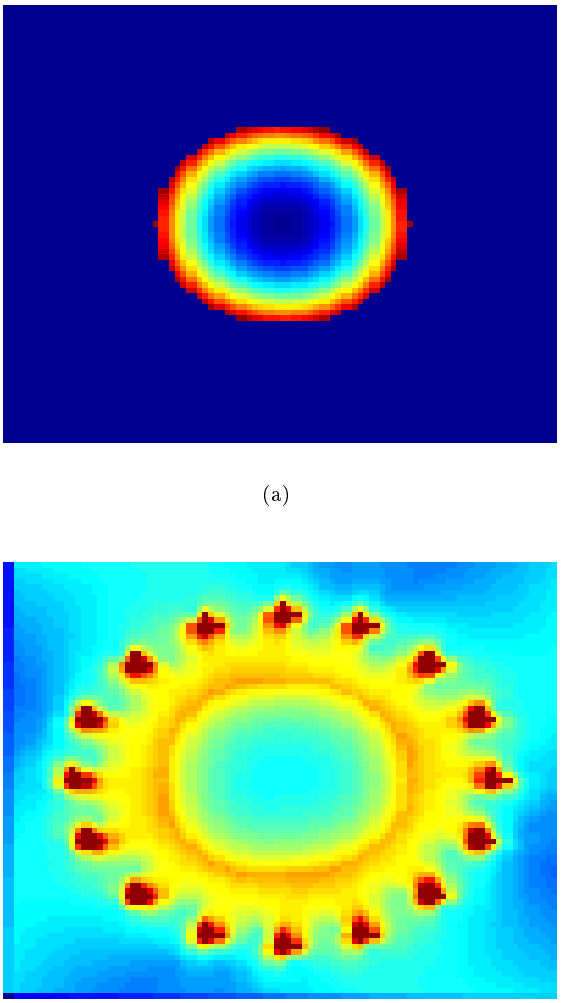

(a)

(b)

Fig. 4. The SAR (a) and the magnetic field (b) of a loaded circular birdcage coil.

The loading of the coil decreases the field homogeneity. However, the magnetic field is fairly constant over the imaged region. The highest magnetic and electric field inside the 'body' are close to the surface. The SAR map shows the highest intensity (2.13 W/kg) at the surface also.

D. Loaded Coil and Catheter

In the last experiment an infinitely thin catheter was placed in the center of the grid. The catheter had a length of 0.21 m and was aligned parallel to the x-axis in the center of the grid. The catheter was numerically implemented by setting the E_z component to zero. The results of this simulation are shown in Figure (5).

In these images we see, that the electric field is zero at the location of the catheter and (a horizontal bar in the center). The magnetic field is disturbed significantly by the presence of the catheter. High amplitudes are present at each end of the catheter. The SAR has a higher maximum value (2.30 W/kg) compared to the loaded coil without a catheter. However, the SAR integrated over the whole volume is slightly smaller.

V. Discussion

The results of the circular and linear polarized field distributions do agree with the results reported in other publications (see especially [18] for lots of color images). The FDTD algorithm solves the electromagnetic problem as a function of time. Generated movie loops of the field components of a birdcage coil can be helpful for educational purposes.

The result show that th insertion of a metallic catheter does disturb the fields. In reality, the cathter does not extend into the third dimension like a thin metallic sheet (this is what we imply with the 2D simulation). The catheter would not have two ends in the body. The observation from other studies, that the temperature increases at the tip of the catheter can not be explained by the results of this study.

There are a variety of possible modifications and extensions to the implemented numerical simulations. The transition from 2D to 3D would give more accurate results but also increase the computational effort (implementation + run time). A human model with classified tissues would also result in a more realistic simulation. Hot spots are likely to occur in the human body and they are detectable if the resolution of the model is sufficient. The current distribution in the coil can be modeled more accurate, e.g. with a lumped circuit approach. Also, the very small geometry of the catheter coil can be modeled more precisely. This would require a grid with varying resolutions over the covered area. The boundary condition can be improved from a MUR RBC to the perfect matched layer (PML) boundary condition, which is numerically more accurate. With such a 'perfect' simulation, it may be possible to optimize the antenna design for the catheters.

Acknowledgments

The author would like to acknowledge the suggestions of Professor Susan Hagness, even though he has not been able to implement all of the creative ideas. This may leave some opportunities for motivated students who search for a Ph.D. thesis project.

References

[1] S. Hagness, "ECE 906 - Special Topics in Electrodynamic Fields: Computational Electrodynamics," Course Notes, University of Wisconsin-Madison, Dept. of Electrical and Computer Engineering, 1998.

[2] A. Taflove, *Computational Electrodynamics - The Finite Difference Time-Domian Method.* Boston, MA: Artech House, 1995.

[3] A. Abragam, *Principles of Nuclear Magnetism.* Oxford, UK: Oxford University Press, 1994.

[4] D. R. Bailes and D. J. Bryant, "NMR imaging," *Contemporary Physics*, vol. 25, no. 5, pp. 441–75, 1984.

[5] E. Krestel, *Imaging Systems for Medical Diagnostics.* Berlin: Siemens, 1990.

[6] C. Hayes, W. A. Edelstein, J. F. Schenck, O. M. Mueller, and M. Eash, "An efficient highly homogeneous radiofrequency coil for whole-body nmr imaging at 1.5 t," *Journal of Magnetic Resonance*, vol. 63, pp. 622–28, 1985.

[7] C. E. Hayes, W. A. Edelstein, and J. F. Schenck, "Radiofrequency coils," in *NMR in Medicine* (S. R. Thomas and R. L. Dixon, eds.), pp. 142–165, College Park, MD: American Association of Physicists in Medicine, 1985.

[8] J. F. Schenck, "Radiofrequency coils: types and characteristics," in *The Physics of MRI* (P. Sprawls and M. J. Bronskill, eds.), pp. 98–134, College Park, MD: American Association of Physicists in Medicine, 1992.

[9] J. R. MacFall, "Hardware and coils for MR imaging," in *Categorical Course in Physics: The Basic Physics of MR Imaging* (S. J. Riederer and M. L. Wood, eds.), pp. 41–57, Radiolocical Society of North America, 2021 Spring Road, Suite 600, Oak Brook, IL 60523: RSNA Publications, 1997.

[10] C. L. Dumoulin, S. P. Souza, and R. D. Darrow, "Real time position monitoring of invasive devices using magnetic resonance," *Magnetic Resonance in Medicine*, vol. 29, pp. 411–15, 1993.

[11] O. Ocali and E. Atalar, "Intravascular magnetic resonance imaging using a loopless catheter antenna," *Magnetic Resonance in Medicine*, vol. 37, pp. 112–18, 1997.

[12] M. E. Ladd, P. Ehrhardt, J. F. Debatin, E. Hofmann, P. Boesiger, G. K. von Schulthess, and G. C. McKinnon, "Guidwire antennas for mr fluoroscopy," *Magnetic Resonance in Medicine*, vol. 37, pp. 891–97, 1997.

[13] D. J. Schaefer, "Bioeffects of MRI and patient safety," in *The Physics of MRI* (P. Sprawls and M. J. Bronskill, eds.), pp. 387–421, College Park, MD: American Association of Physicists in Medicine, 1992.

[14] T. K. F. Foo, C. E. Hayes, and Y. W. Kang, "An analytical model for design of rf resonators for MR body imaging," *Magnetic Resonance in Medicine*, vol. 21, pp. 165–77, 1991.

[15] T. K. F. Foo, C. E. Hayes, and Y. W. Kang, "Reduction of rf penetration effects in high field imaging," *Magnetic Resonance in Medicine*, vol. 23, pp. 287–301, 1992.

[16] J. Jin, G. Shen, and T. Perkins, "On the field inhomogeneity of a birdcage coil," *Magnetic Resonance in Medicine*, vol. 32, pp. 418–22, 1994.

[17] D. Simunic, P. Wach, W. Renhart, and R. Stollberger, "Spatial distribution of high-frequency electromagnetic energy in human head during MRI: Numerical results and measurements," *IEEE Transactions on Biomedical Engineering*, vol. 43, pp. 88–94, 1996.

[18] J. Jin and J. Shen, "On the sar and field inhomogeneity of birdcage coils loaded with the human head," *Magnetic Resonance in Medicine*, vol. 38, pp. 953–63, 1997.

[19] J. Felmlee, D. Hokanson, and W. Perkins, "Real time evaluation of EKG electrode heating during mri at 1.5 t," in *International Society for Magnetic Resonance in Medicine*, p. 1226, ISMRM, 1995.

[20] R. Buchli, P. Boesiger, and D. Meier, "Heating effects of metallic implants by MRI examinations," *Magnetic Resonance in Medicine*, vol. 7, pp. 225–61, 1988.

[21] M. E. Ladd, G. G. Zimmermann, H. H. Quick, J. F. Debatin, P. Boesiger, G. K. von Schulthess, and G. C. McKinnon, "Guidwire antennas for mr fluoroscopy," *Journal of Magnetic Resonance Imaging*, vol. 8, pp. 220–25, 1998.

[22] S. E. Maier, S. Wildermuth, R. D. Darrow, R. D. Watkins, J. F. Debatin, and C. L. Dumoulin, "Safety of MR tracking catheters," in *International Society for Magnetic Resonance in Medicine*, p. 497, ISMRM, 1995.

[23] C. Gabriel, S. Gabriel, and E. Corthout, "The dielectric properties of biological tissues: I. Literature survey," *Phys. Med. Biol.*, vol. 41, pp. 2231–49, 1996.

[24] C. Gabriel, R. W. Lau, and S. Gabriel, "The dielectric properties of biological tissues: Ii. Measurements in the frequency range 10 Hz to 20 GHz," *Phys. Med. Biol.*, vol. 41, pp. 2251–69, 1996.

[25] C. Gabriel, R. W. Lau, and S. Gabriel, "The dielectric properties of biological tissues: Iii. parametric models for the dielectric spectrum of tissues," *Phys. Med. Biol.*, vol. 41, pp. 2271–93, 1996.

[26] J. Shen, Z. Feng, and J. Jin, "Numerical simulation of sar and b_1-field inhomogeneity of shielded rf coils loaded with the human head," *IEEE Transactions on Biomedical Engineering*, vol. 45, pp. 650–659, 1998.
[27] J. A. Sorenson, "The Physics of MRI," Depts. of Medical Physics and Radiology, University of Wisconsin-Madison, 1998.
[28] G. H. Glover, C. Hayes, and N. J. Pelc, "Comparison of linear and circular polarization for magnetic resonance imaging," *Journal of Magnetic Resonance*, vol. 64, pp. 255–70, 1985.

Fig. 6:

OLIVER WIEBEN received his Vordiplom in Electrical Engineering at the Universität Hannover, Germany in 1993, his Diplom at the Universität Karlsruhe, Germany in 1998 and his MS degree at the University of Wisconsin, Madison in December 1996, where he is a Ph.D. student in Electrical and Computer Engineering by now. His research is related to biomedical engineering applications involving digital signal processing, image processing, and pattern recognition. He contributed to the development of the MEET-Man Project at the Universität Karlsruhe, where a detailed finite element model of the human body was created based on tissue-classified MRI scans. The work for the MS thesis focussed on automated ECG interpretation with a filter bank approach. His current research at the Departments of Medical Physics and Radiology is related to time resolved and contrast enhanced Magnetic Resonance Angiography.
Mr. Wieben is a member of the Institute of Electrical and Electronics Engineers (IEEE), the American Association of Medical Physicists (AAMP), and the International Society for Magnetic Resonance in Medicine (ISMRM).

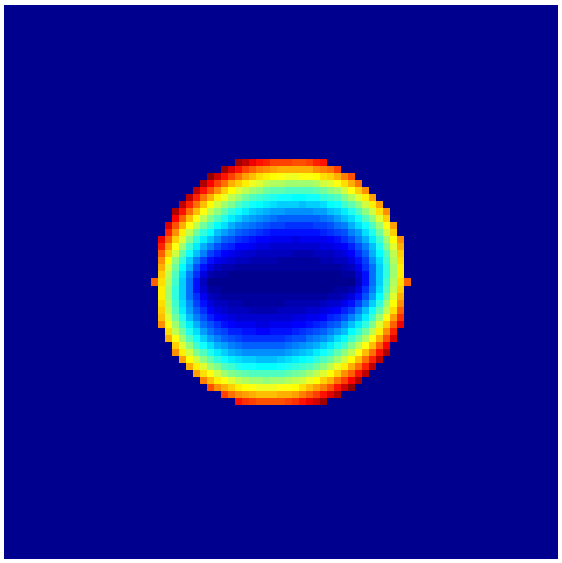

(a)

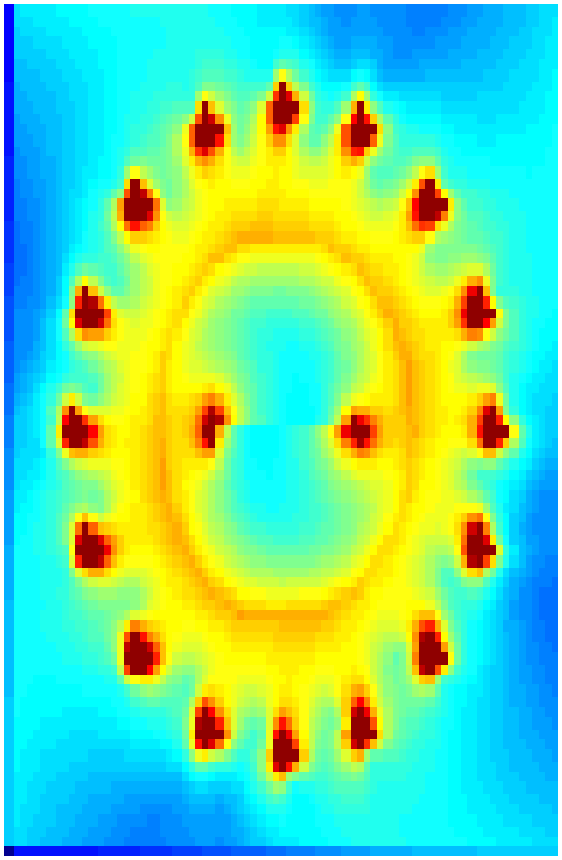

(b)

Fig. 5. The SAR map (a) and the magnetic field (b) of a loaded circular birdcage coil in the presence of a catheter.